Superscripts

~ = conduction value
′ = variation from value at mean fluid temperature

LITERATURE CITED

1. Abbott, M. R., *Quart. J. Mech. Appl. Math.*, **17**, 471 (1964).
2. Aziz, K., and J. D. Hellums, *Phys. Fluids*, **10**, 314 (1967).
3. Brian, P. L. T., *AIChE J.*, **7**, 367 (1961).
4. Deardorff, J. W., *J. Atmos. Sci.*, **21**, 419 (1964).
5. Douglas, J., Jr., *Num. Math.*, **4**, 41 (1962).
6. Elder, J. W., *J. Fluid Mech.*, **24**, 823 (1966).
7. Fromm, J. E., *Phys. Fluids*, **8**, 1757 (1965).
8. Hellums, J. D., Ph.D. thesis, Univ. Michigan, Ann Arbor (1963).
9. Lemlich, R., and L. Crawford, *Ind. Eng. Chem. Fundamentals*, **1**, 260 (1962).
10. Liu, C. Y., W. K. Mueller, and F. Landis, *Intern. Develop. Heat Transfer*, Part IV, 976 (1961).
11. Noble, J. J., Ph.D. thesis, Massachusetts Inst. Technol., Cambridge (1968).
12. Piacsek, S. A., Ph.D. thesis, Massachusetts Inst. Technol., Cambridge (1968).
13. Samuels, M. R., Ph.D. thesis, Univ. Michigan, Ann Arbor (1965).
14. ———, *Phys. Fluids*, **11**, 1889 (1968).
15. Schwab, T. H., M.S. thesis, Univ. Toledo, Ohio (1968).
16. Wilkes, J. D., Ph.D. thesis, Univ. Michigan, Ann Arbor (1963).
17. Williams, G. P., *J. Atmos. Sci.*, **24**, Part 1, 144 (1967).
18. ———, *ibid.*, Part 2, 162 (1967).

Manuscript received October 10, 1968; revision received April 14, 1969; paper accepted April 16, 1969.

Numerical Treatment of Fully Developed Laminar Flow in Helically Coiled Tubes

L. C. TRUESDELL, JR., and R. J. ADLER
Case Western Reserve University, Cleveland, Ohio

Laminar flow in helically coiled tubes is treated numerically. Fully developed axial and secondary velocities are calculated for both circular and elliptical cross sections. Only closely wrapped helices, that is, helices with modest pitch, are considered. Ten solutions with Deans numbers up to 200 have good accuracy. Two additional solutions with Deans numbers up to 280 are approximate.

Secondary flow, that is, flow perpendicular to the main direction of flow, occurs whenever fluid passes through a curved tube or channel. The phenomenon is caused by centrifugal forces, and can be readily explained by reference to Figure 1, the cross section of a helically coiled tube. Near the tube's center the axial velocity is greatest, causing centrifugal forces to act most strongly. Fluid is thrown outward and replaced by recirculating fluid which flows inward along the walls. In laminar and turbulent flow two strong symmetrical patterns are normally established.

Certain important effects are caused by secondary flow. For example, the snaking or meandering of rivers flowing across alluvial plains is due to secondary flow (*1, 2*). Superior heat transfer characteristics are possessed by coiled tube heat exchangers (*3* to *5*). Secondary flow stabilizes laminar flow, transition Reynolds numbers of 6,000 to 8,000 being characteristic of helically coiled tubes (*6*). Secondary flow markedly reduces axial dispersion, an effect of interest in chromatography and chemical reactor design (*7*). These effects and others are described in a literature which dates back almost 100 yr. A listing of important references through 1964 has been compiled (*7*).

A numerical treatment of fully developed laminar flow, including secondary flow, is reported here for helically coiled tubes. The treatment is based on a finite-difference approximation to the governing continuous equations and is valid over a greater range of operating conditions than previous analytical solutions (*8* to *11*). Analytical solutions to date have been limited because they are based on expressing velocity and pressure in a power series in a/r, where a is the radius of the tube and r is the radius of curvature of the helix. Because of algebraic complexity, it has been practical to retain only terms of first order. The resulting analytical solutions have been valid only for small values, perhaps up to two or three, of a dimensionless criterion called the Deans number, $N_{Re}(a/r)^{1/2}$. Numerical solutions having good accuracy are presented in this paper for Deans numbers up to approximately 200.

The work reported encompasses both round and elliptical cross sections. Incompressible, fully developed flow is assumed. Only the practically important case of small pitch $h/2\pi r$ is considered (see Figure 2 for the definition of h).

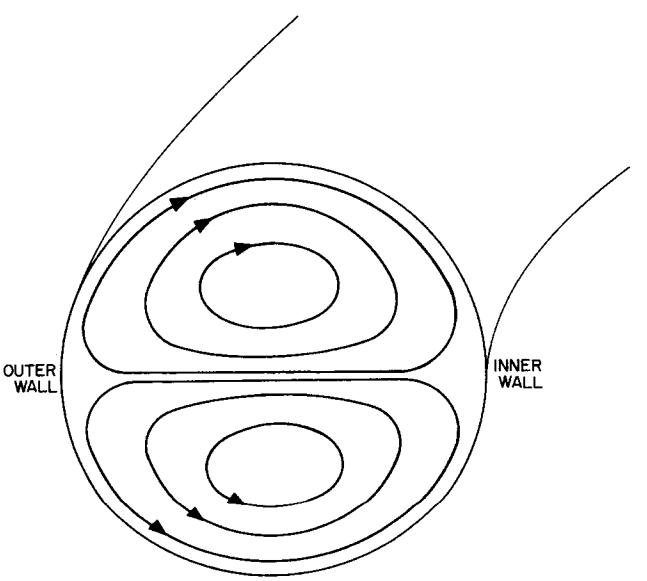

Fig. 1. Secondary flow patterns in the cross section of a helically coiled tube.

L. C. Truesdell, Jr., is with Shell Development Company, Emeryville, California.

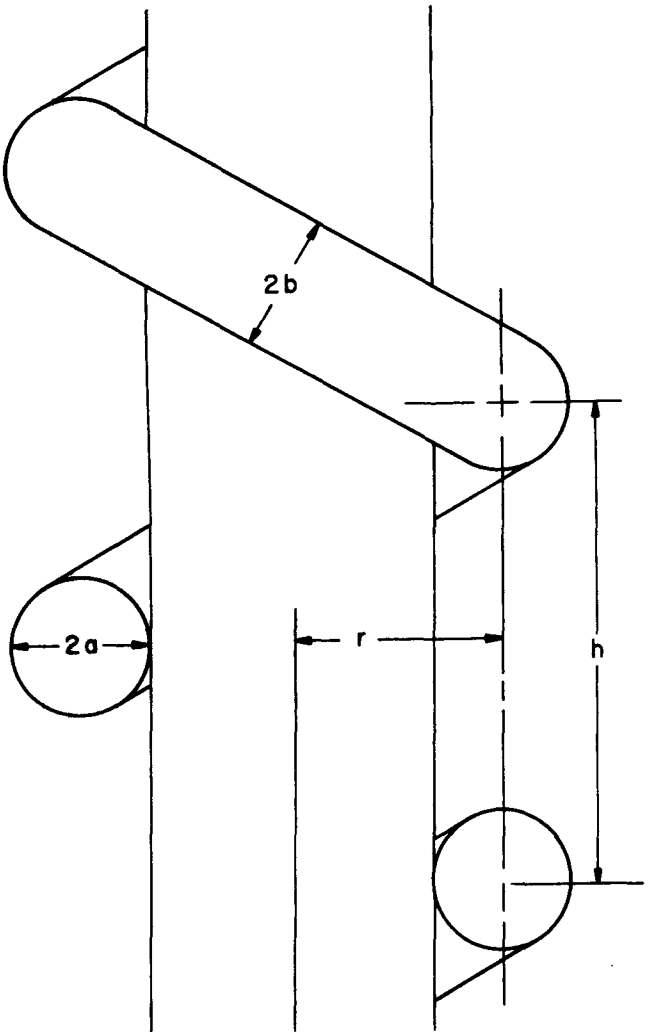

Fig. 2. Geometrical variables.

Results for secondary flow, downstream velocity, and pressure drop are reported for twelve cases in tables and graphs. Comparisons are made wherever possible with others' experimental data and analytical solutions.

CONTINUOUS EQUATIONS

The geometrical variables describing helically coiled tubes are defined in Figure 2. An elliptical cross section is described by semiaxes a and b. The perpendicular distance from the mandrel axis to the center of the tube's cross section is denoted by r. The distance parallel to the mandrel axis between corresponding points on adjacent coils is h.

For simplicity, the helically coiled tube is treated as a torus ($h = 0$) defined by Figure 3. Later it will be argued that the main effects of moderate values of pitch $h/2\pi r$ can be incorporated by a simple correction in the value of r associated with the torus solution. The rectangular coordinates in the cross-sectional plane are x and y. An orthogonal curved coordinate z coincides with the circular axis of the torus.

The Navier-Stokes and continuity equations governing this case have been stated in dimensionless form by Cuming (*10*). Dimensional and dimensionless quantities are related as follows. The velocities u, v, and w in the x, y, and z directions are related to dimensionless velocities U, V, and W by $u = \nu U/a$, $v = \nu V/a$, and $w = \nu W/a$, where $\nu = \mu/\rho$ is the kinematic viscosity. Distances are related by $x = aX$, $y = bY$, and $z = aZ$. Defining an ellipticity $\lambda = b/a$ permits y to be expressed as $y = \lambda aY$. The pressures are related by $p = \rho\nu P/a^2$ and the times by $t = a^2T/\nu$. Dropping velocity derivatives in the Z direction which are zero for fully developed flow, the Navier-Stokes and continuity equations are

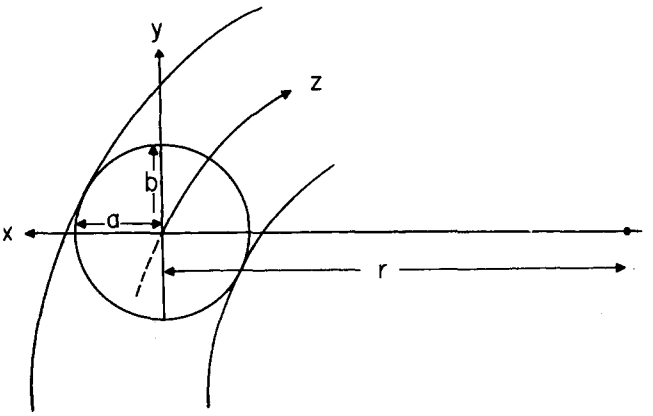

Fig. 3. Torus.

$$\frac{\partial U}{\partial T} + U\frac{\partial U}{\partial X} + \frac{V}{\lambda}\frac{\partial U}{\partial Y} - \frac{(a/r)W^2}{[1+(a/r)X]} = -\frac{\partial P}{\partial X} + \frac{1}{\lambda^2}\frac{\partial^2 U}{\partial Y^2} - \frac{1}{\lambda}\frac{\partial^2 V}{\partial X \partial Y} \quad (1a)$$

$$\frac{\partial V}{\partial T} + U\frac{\partial V}{\partial X} + \frac{V}{\lambda}\frac{\partial V}{\partial Y} = -\frac{1}{\lambda}\frac{\partial P}{\partial Y} + \frac{\partial^2 V}{\partial X^2} - \frac{1}{\lambda}\frac{\partial^2 V}{\partial X \partial Y} + \frac{(a/r)}{[1+(a/r)X]}\cdot\left(\frac{\partial V}{\partial X} - \frac{1}{\lambda}\frac{\partial U}{\partial Y}\right) \quad (1b)$$

$$\frac{\partial W}{\partial T} + U\frac{\partial W}{\partial X} + \frac{V}{\lambda}\frac{\partial W}{\partial Y} + \frac{(a/r)UW}{[1+(a/r)X]} = \frac{-1}{[1+(a/r)X]}\frac{\partial P}{\partial Z} + \frac{\partial^2 W}{\partial X^2} + \frac{1}{\lambda^2}\frac{\partial^2 W}{\partial Y^2} + \frac{(a/r)}{[1+(a/r)X]}\frac{\partial W}{\partial X} - \frac{(a/r)^2 W}{[1+(a/r)X]^2} \quad (1c)$$

$$\frac{\partial}{\partial X}([1+(a/r)X]\,U) + \frac{1}{\lambda}\frac{\partial}{\partial Y}([1+(a/r)X]\,V) = 0 \quad (1d)$$

The boundary conditions are zero velocity at the walls and symmetry with respect to the X axis:

$$\left.\begin{aligned} U &= 0 \\ V &= 0 \\ W &= 0 \end{aligned}\right\} \text{ at } X^2 + Y^2 - 1 = 0$$

$$\text{and} \quad V = 0 \quad \text{at} \quad Y = 0$$

The pressure gradient $\partial P/\partial Z$ in (1c) is easily shown to be a constant by differentiating Equations (1a), (1b), and (1c) with respect to Z and by making use of the fact that all downstream (Z direction) velocity derivatives are zero.

The pressure gradients $\partial P/\partial X$ and $\partial P/\partial Y$ can be eliminated by differentiating (1a) with respect to λY, by differentiating (1b) with respect to X, and by subtracting. This yields a third-order equation in U, V, and W. The only pressure term remaining in the system of equations is the constant downstream pressure gradient $\partial P/\partial Z$.

Since the continuity Equation (1*d*) is two dimensional, it is attractive to eliminate it by introducing a stream function Ψ defined by

$$V = \frac{1}{[1 + (a/r)X]} \frac{\partial \Psi}{\partial X} \tag{2a}$$

$$U = \frac{-1}{\lambda[1 + (a/r)X]} \frac{\partial \Psi}{\partial Y} \tag{2b}$$

By using a simplified notation where $A = a/r$ and $B = 1 + (a/r)X$, the governing equations become

$$\frac{-2A}{\lambda} W \frac{\partial W}{\partial Y} + \frac{1}{\lambda^4} \frac{\partial^4 \Psi}{\partial Y^4} + \frac{2}{\lambda^2} \frac{\partial^4 \Psi}{\partial Y^2 \partial X^2} + \frac{\partial^4 \Psi}{\partial X^4}$$
$$- \frac{2A}{\lambda^2 B} \frac{\partial^3 \Psi}{\partial X \partial Y^2} - \frac{2A}{B} \frac{\partial^3 \Psi}{\partial X^3} + \frac{3A^2}{B^2} \frac{\partial^2 \Psi}{\partial X^2} - \frac{3A^3}{B^3} \frac{\partial \Psi}{\partial X}$$
$$+ \frac{1}{\lambda B} \frac{\partial^3 \Psi}{\partial X^3} \cdot \frac{\partial \Psi}{\partial Y} - \frac{1}{\lambda B} \cdot \frac{\partial^3 \Psi}{\partial X^2 \partial Y} \cdot \frac{\partial \Psi}{\partial X} + \frac{1}{\lambda^3 B} \frac{\partial^3 \Psi}{\partial X \partial Y^2}$$
$$\cdot \frac{\partial \Psi}{\partial Y} - \frac{1}{\lambda^3 B} \frac{\partial^3 \Psi}{\partial Y^3} \cdot \frac{\partial \Psi}{\partial X} + \frac{A}{\lambda B^2} \frac{\partial^2 \Psi}{\partial X \partial Y} \cdot \frac{\partial \Psi}{\partial X}$$
$$- \frac{3A}{\lambda B^2} \frac{\partial^2 \Psi}{\partial X^2} \cdot \frac{\partial \Psi}{\partial Y} - \frac{2A}{B^2 \lambda^3} \frac{\partial^2 \Psi}{\partial Y^2} \cdot \frac{\partial \Psi}{\partial Y} + \frac{3A^2}{\lambda B^3} \frac{\partial \Psi}{\partial X}$$
$$\cdot \frac{\partial \Psi}{\partial Y} = \frac{1}{\lambda^2} \frac{\partial^3 \Psi}{\partial Y^2 \partial T} + \frac{\partial^3 \Psi}{\partial X^2 \partial T} - \frac{A}{B} \frac{\partial^2 \Psi}{\partial X \partial T} = 0 \tag{3a}$$

and

$$\frac{1}{\lambda B} \frac{\partial \Psi}{\partial Y} \cdot \frac{\partial W}{\partial X} - \frac{1}{\lambda B} \frac{\partial \Psi}{\partial X} \cdot \frac{\partial W}{\partial Y} + \frac{A}{\lambda B^2} \frac{\partial \Psi}{\partial Y} \cdot W$$
$$- \frac{1}{B} \frac{\partial P}{\partial Z} + \frac{\partial^2 W}{\partial X^2} + \frac{1}{\lambda^2} \frac{\partial^2 W}{\partial Y^2} + \frac{A}{B} \frac{\partial W}{\partial X} - \frac{A^2}{B^2} W$$
$$= \frac{\partial W}{\partial T} = 0 \tag{3b}$$

with boundary conditions

$$\left.\begin{array}{l} \dfrac{\partial \Psi}{\partial X} = 0 \\ \dfrac{\partial \Psi}{\partial Y} = 0 \\ \Psi = 0 \\ W = 0 \end{array}\right\} \text{at } X^2 + Y^2 - 1 = 0 \qquad \left.\begin{array}{l} \\ \\ \\ \\ \Psi = 0 \end{array}\right\} \text{at } Y = 0 \tag{3c}$$

The time derivatives on the right-hand side of (3*a*) and (3*b*) are, of course, equal to zero for fully developed flow. They are included here only because they are later used in developing a computational algorithm. It should be remembered that Equations (3*a*), (3*b*), and (3*c*) apply rigorously only for a torus, that is $h/2\pi r = 0$, the limiting case of a helically coiled tube with zero pitch.

There are two effects of finite pitch. First, there is an increase in the radius of curvature at all points in the tube cross section. Second, centrifugal forces cease to act solely in the cross-sectional plane. The first effect is discussed and analyzed in Appendix A. It is concluded that, to a high degree of approximation, the increase in radius of curvature may be compensated for by replacing the radius r in terms A and B in Equations (3*a*) and (3*b*) by $r\left[1 + \left(\frac{h}{2\pi r}\right)^2\right]$. Since for most reasonable geometries the pitch $h/2\pi r$ would rarely exceed about 0.2, this correction is seen to be modest. The second effect acts to distort the symmetry assumed about the X axis; fluid on one side of the X axis flows downstream more rapidly, and fluid on the other side more slowly, than in a torus. This effect has not been analyzed mathematically. However, experiments performed in our laboratories with tracers in helically coiled tubes of moderate pitch ($h/2\pi r \simeq 0.03$) and curvature ($a/r \simeq 0.09$) have shown differences in downstream velocity between the two halves of the cross section of only about 1%. It is therefore concluded that this second effect is quite small for moderate pitch and curvature values.

COMPUTATIONAL ALGORITHM

Continuous Equations (3*a*) and (3*b*), being coupled, of high order and containing nonlinearities in the form of products of derivatives of the dependent variables Ψ and W do not lend themselves to analytical solution. For this reason a numerical approach is used, specifically a relaxation technique. The computational algorithm is based on approximating spatial derivatives by central differences and time derivatives by forward differences. The time derivative terms are used to guide the iterative relaxation of $\Psi_{m,n}$ and $W_{m,n}$ from a first estimate to values which satisfy closely the steady state versions of Equations (3*a*) and (3*b*). An alternate view of the computations is that they march forward in time from an initial unsteady state toward the steady state, which is the desired solution.

The left-hand sides of Equations (3*a*) and (3*b*) are approximated to fourth order or higher accuracy by standard central differences of the type attributed to Stirling, except for the terms $\frac{\partial^2 W}{\partial X^2} + \frac{1}{\lambda^2} \frac{\partial^2 W}{\partial Y^2}$ appearing in (3*b*) which were approximated to third-order accuracy by a nine point formula (*12*). Let $R\Psi_{m,n}$ and $RW_{m,n}$ be the finite difference values of the left-hand sides of (3*a*) and (3*b*), respectively, at mesh point m,n. Let $\delta\Psi_{m,n}$ and $\delta W_{m,n}$ be increments in $\Psi_{m,n}$ and $W_{m,n}$, respectively, associated with the time increment δt. Then, Equations (3*a*) and (3*b*) become

$$\frac{1}{\lambda^2} \frac{\partial^2 (\delta\Psi_{m,n})}{\partial Y^2} + \frac{\partial^2 (\delta\Psi_{m,n})}{\partial X^2} - \frac{A}{B} \frac{\partial (\delta\Psi_{m,n})}{\partial X}$$
$$= \delta T \cdot R\Psi_{m,n} \tag{4a}$$

$$\delta W_{m,n} = \delta T \cdot RW_{m,n} \tag{4b}$$

with boundary conditions

$$\left.\begin{array}{l} \dfrac{\partial \delta\Psi}{\partial X} = \dfrac{\partial \delta\Psi}{\partial Y} = 0 \text{ and } \delta\Psi_{m,n} = 0 \\ \qquad\qquad\qquad\qquad \text{at } X^2 + Y^2 - 1 = 0 \\ \delta\Psi_{m,n} = 0 \quad \text{at} \quad Y = 0 \end{array}\right\} \tag{4c}$$

Equation (4*b*) gives the increments $\delta W_{m,n}$ explicitly. Equation (4*a*), which gives the increments $\delta\Psi_{m,n}$ implicitly, is a standard, linear, boundary-value problem. This equation is solved by a standard point relaxation technique. Ten sweeps of the field were employed, with simultaneous updating of the values of $\delta\Psi_{m,n}$ after each sweep. Values of $\delta\Psi_{m,n}$ resulting from the tenth sweep were stored as initial estimates for the first sweep at the beginning of the next time period.

TABLE 1. SUMMARY OF COMPUTED SOLUTIONS

Case number	$\frac{\partial P}{\partial Z}$	λ	a/r	N_{Re}*	N_{De}*	$\frac{fs^{**}}{fc}$
1	−40.0	1.000	0.0100	10.0	1.0	1.000
2	−800.0	1.000	0.0100	192.4	19.24	1.040
3	−800.0	1.000	0.0500	168.4	37.66	1.187
4	−800.0	1.000	0.1000	156.0	49.3	1.282
5	−8,000.0	1.000	0.0100	1,229.0	122.9	1.625
6+	−8,000.0	1.000	0.0500	996.+	223.+	2.01+
7+	−8,000.0	1.000	0.1000	934.+	295.+	2.15+
8	−1,271.6	0.685	0.1167	134.2	41.7	1.60 (1.21)
9	−409.6	1.460	0.0800	136.6	42.5	1.57 (1.19)
10	−800.0	2.000	0.1000	286.7	102.0	3.46 (1.41)
11	−800.0	1.460	0.0800	234.3	71.9	1.79 (1.35)
12	−800.0	0.500	0.1000	48.4	11.9	3.07 (1.04)

* For elliptical cases (runs 8 through 12), Reynolds and Deans numbers are based on hydraulic radii.
** Flux ratios are based on fs being calculated for straight circular tubes of the same circumference. Flux ratios in parentheses for elliptical cases (cases 8 through 12) are based on fs being calculated for straight elliptical tubes with the same cross section.
† Approximate solutions only. Continued slow oscillations prevented complete convergence to the steady state.

A square mesh was employed, with twenty equally spaced points per diameter. Because of symmetry about the X axis, it is necessary to compute the flow explicitly over only a semicircular cross section. Superimposing of a square grid upon a semicircular cross section complicates the approximation of the boundary conditions. To avoid special formulas at the boundary, a number of fictitious grid points outside the actual cross section were used. Of the 258 mesh points employed, ninety-eight were outside of the boundary of the semicircular cross section. The values of the stream function and downstream velocity at these external grid points were determined by Taylor series extrapolations centered on the boundary. Stream function values were estimated by using fourth-order Taylor series while velocity values were estimated with third-order series. The majority of these Taylor series were one dimensional. Certain points within the boundary, but very close to it, were found to be strongly influenced by external points. These points, termed *selvedge points*, were occasionally smoothed by means of two-dimensional Taylor series carried through second-order terms.

NUMERICAL RESULTS

Twelve cases were treated, each corresponding to a particular combination of system variables $\partial P/\partial Z$, λ, and a/r. A list of these cases appears in Table 1 along with the resulting Reynolds and Deans numbers calculated from the solutions. Also listed is the ratio of the volumetric flux in a straight pipe to the flux in the curved system fs/fc at equal values of $\partial P/\partial Z$. Downstream velocities and cross-sectional stream functions are reported by Figures 6 through 32 in Appendix B* as surfaces over the semicircular field. Detailed numerical values are also available (*12*).

From these computed solutions it is possible to make observations about the dependence of the downstream velocity profile and stream function on the system variables. Case 1 is within the limits of Cuming's perturbation solution (*10*). It shows a weak secondary flow pattern almost symmetrically located in the center of the semicircular field. At such low Deans numbers the effect of curvature on the downstream velocity profile is negligible.

As the pressure gradient and curvature are increased, the secondary flow patterns become more intense. The centers of the secondary vortices move outward in the positive X direction and upward and downward in the Y direction, leaving a relatively stagnant region near $X = -1$, $Y = 0$. At still higher Deans numbers the center of the secondary flow patterns shift back toward $X = 0$ and move further upward and downward in the Y direction. The stagnant region near $X = -1$, $Y = 0$ persists.

With increasing pressure gradient and curvature, the downstream velocity profile is gradually distorted from a paraboloid. The region of maximum axial velocity moves toward the outer wall, that is, in the positive X direction, and the flow, as compared with the flux in a straight pipe at the same pressure gradient, is diminished. As the Deans number increases, the downstream velocity profile approaches a trapezoidal shape. In the center region, it is almost linear when cut by planes of constant Y values.

Variables in cases 8 and 9 were chosen to study the effects of distorting the cross section of a tube from a circle to an ellipse. These runs are essentially a duplication of the conditions in case 4 with, however, the cross section distorted from a circle to an ellipse. In these three cases the tube wall has the same circumference and there are equal dimensional pressure gradients, fluid properties, and center-line curvatures. In case 8 the cross section major axis is oriented parallel to the radius of curvature, while in case 9 the major axis is perpendicular. Distortion in the axes in each case amounts to about 20% of the circular cross section radius.

As shown in the last column of Table 1, the flow resistance of cases 8 and 9 is greater than case 4. This is due to a reduction in cross-sectional area (cases 4, 8, and 9 have the same circumference); note that fs/fc for elliptical tubes is less than fs/fc for circular tubes (the elliptical flux ratio appears parenthetically in Table 1). It is, perhaps, not surprising that the relative resistance is less in a system of elliptical tubes considering the lower Deans numbers involved.

Further consideration of cases 8 and 9 indicates that there is slightly more flux diminution when the major axis is parallel to the helix radius of curvature. The secondary flow intensity is also higher, in fact greater than for circular cross sections. This result is in agreement with the prediction of Cuming (*10*) for much lower Deans numbers. It

* Material has been deposited as document 01202 with the ASIS National Auxiliary Publications Service, c/o CCM Information Sciences, Inc., 22 W. 34th St., New York 10001 and may be obtained for $2.00 for microfiche or $5.00 for photocopies.

appears, then, that stronger secondary flows can be generated by distorting the cross section into an ellipse with its major axis parallel to the helix radius of curvature. This increased secondary circulation arises, of course, at the expense of additional pressure gradient.

It was hoped that solutions could be obtained for increasingly high Deans numbers, but an upper limit was encountered due to oscillatory tendencies of solutions above Deans numbers of approximately 200. In cases 6 and 7, the only two performed for Deans numbers above 200, the stream function and velocity values converged rather rapidly to the region of the expected solution but then began to slowly oscillate in a nonperiodic fashion and failed to converge further. During the course of these oscillatory iterations the velocity values varied about 10%, while the stream function oscillated as much as 15%. This effect was most pronounced in case 7, at a Deans number of 295. About 450 iterations were performed without appreciably reducing the oscillations, and it was concluded that convergence could not be obtained.

Although it is likely that the oscillation experience was caused by deficiencies in the simple numerical method employed, it should perhaps be noted that helically coiled systems have a more gradual transition from laminar to turbulent flow than do straight tubes. Taylor (*6*) injected dye into a helically coiled tube and noted: ".... the flow was steady up to a certain speed. At this speed the color band began to vibrate in an irregular manner, but still seemed to retain its identity through at least one whole turn of the helix. This indicates that the unsteadiness was not at first of a type which gives rise to diffusion of momentum by eddies." Of course, it is impossible to draw a direct analogy between the mathematical and physical systems, and the unsteadiness is more likely a consequence of the numerical method employed.

One attempt to calculate under substantially more severe conditions ($\partial P/\partial Z = 40{,}000$, $a/r = 0.1$, and $\lambda = 1.0$) failed completely owing to divergence in the region of the boundary. However, it is too much to hope that these conditions could be handled, since Adler's analytical analysis (*14*) predicts a boundary-layer thickness for this case of approximately one-fourth of the grid spacing. For the sake of completeness, it should be reported that the computer employed was the Burroughs 220 (5,000 core words, addition time of 185μ sec., average multiplication time of 2,095μ sec.). Each iteration in time required about 2 min. and 20 sec. The number of iterations required for convergence varied from seventeen (case 1) to 193 (case 7). The time step δT varied from 0.002 to 0.0005.

COMPARISONS WITH RESULTS OF OTHERS AND ACCURACY ESTIMATES

Pressure drop vs. flow data measured by many investigators have been correlated in the laminar regime by White (*13*) for tubes of circular cross section. Figure 4 compares the computed runs which have circular cross sections with White's correlation at equal downstream pressure gradients $\partial P/\partial Z$. The agreement is generally good, although case number 7, which showed marked oscillatory behavior as explained previously, is somewhat off the correlation curve. Comparisons with more detailed data cannot be made, since only limited measurements of velocity profiles are available (*14*), and only qualitative observations of secondary flows are reported in the literature.

Case 1 can be compared directly with Cuming's (*10*) series solution for slight curvatures and low Reynolds numbers. Figure 5 shows that stream function solution at the plane $Y = 0.4$ together with selected points from Cuming's solution. The agreement is good, and the velocity profiles, though not presented here, show similar harmony.

Beyond these two comparisons, some a posteriori accuracy estimates can be made by considering the two major sources of errors in the computed solutions, namely truncation errors and incomplete relaxation. Spot checks showed the truncation residuals to be of the same order of magnitude as the relaxation residuals, except for cases 6 and 7 which had relatively large relaxation residuals. The size of the truncation and relaxation residuals indicate that the solutions for Deans numbers of less than 200 are accurate to within 2%. Cases 6 and 7, which showed oscillatory behavior, are less accurate. In case 7, the most unstable, velocity and stream function oscillations were greater than 10%; residual sizes when compared with the axial pressure gradient suggest errors greater than 20%.

SUMMARY

The Navier-Stokes equations have been adapted to describe fully developed laminar flow in helically coiled tubes. The formulation assumes small helix pitch and thus applies rigorously only to closely wrapped helices. Twelve numerical solutions to a finite difference approximation

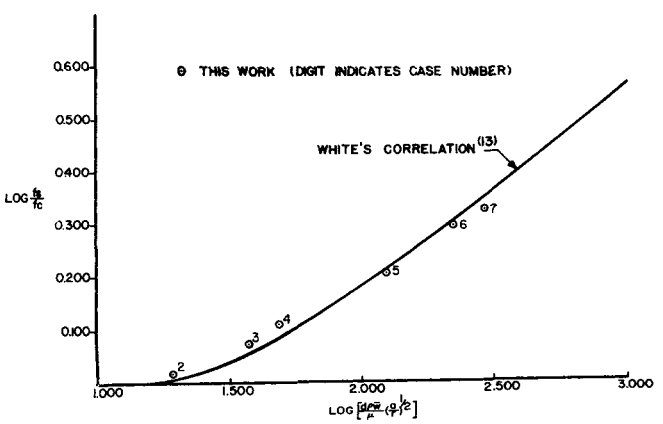

Fig. 4. Flux diminution vs. Deans number.

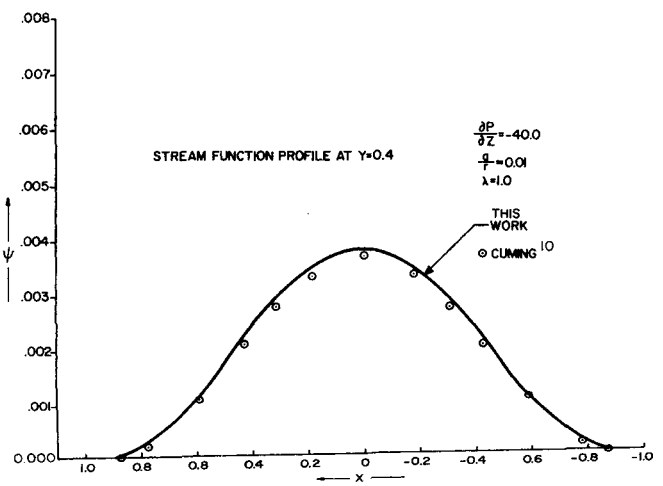

Fig. 5. Comparison with Cuming's solution, stream function.

have been obtained on a digital computer. The solutions have the form of stream function and downstream velocity values at discrete points in the cross section. The twelve solutions cover cases of elliptical and circular cross sections, curvatures from 0.01 to 0.1, and Deans numbers from 1.0 to about 280. Ten of the solutions with Deans numbers less than 200 are accurate to within 2%. Two of the solutions having Deans numbers up to about 280 are approximate.

ACKNOWLEDGMENT

The authors acknowledge the assistance of numerous faculty and students at Case Institute of Technology. Special thanks are due Dr. Merrill Galloway, Jr., for help in checking and deriving the finite difference equations. The Andrew W. Jennings Computing Center is thanked for the extensive use of its facilities. Much appreciated financial support was provided by the National Science Foundation (G14771).

NOTATION

a = elliptical cross section semiaxis in y direction
A = dimensionless curvature = a/r
b = elliptical cross-section semiaxis in x direction
B = function = $1 + (a/r)X$
d = tube diameter, hydraulic diameter in the case of elliptical cross section
f_c = volumetric flux in a helically coiled tube
f_s = volumetric flux in a straight tube
h = distance parallel to helical axis between adjacent turns of a helix
m = discrete X coordinate for finite-difference grid
n = discrete Y coordinate for finite-difference grid
N_{De} = Deans number = $N_{Re}(a/r)^{1/2}$
N_{Re} = Reynolds number, $d\rho w/\mu$
p = fluid pressure, dimensional
P = dimensionless fluid pressure = $a^2p/\rho\nu^2$
r = helical tube center line radius of curvature
R = finite-difference residuals
t = time
T = dimensionless time = $\nu t/a^2$
u = velocity in x direction, dimensional
U = dimensionless velocity in X direction = $a\rho u/\mu$
v = velocity in y direction
V = dimensionless velocity in Y direction = $a\rho v/\mu$
w = velocity in z direction
$\bar{w}$ = average velocity in z direction
W = dimensionless velocity in Z direction = $a\rho w/\mu$
x = dimensional coordinate in cross-sectional plane parallel to center line radius of curvature
X = dimensionless coordinate = x/a
y = spatial coordinate in cross-sectional plane perpendicular to center line radius of curvature
Y = dimensionless coordinate = $y/\lambda a$
z = curved spatial coordinate along tube center line
Z = dimensionless coordinate = z/a

Greek Letters

δ = finite-difference increments
λ = cross-section ellipticity = b/a
μ = fluid viscosity
ν = fluid kinematic viscosity = μ/ρ
ρ = fluid density
Ψ = dimensionless stream function defined by Equations (2a) and (2b)

LITERATURE CITED

1. Thompson, J., *Proc. Roy. Soc. London,* **A25,** 5 (1876).
2. *Ibid.,* **A26,** 356 (1877).
3. Jeschke, D., *Z. Ver. deut. Ing.,* **69,** 1526 (1925).
4. ———, *Z. Ver. deut. Ing. Erganzungscheft,* **24,** 1 (1925).
5. Kreith, F., *Trans. Am. Soc. Mech. Engrs.,* **77,** 1247 (1955).
6. Taylor, G. I., *Proc. Roy. Soc.,* **A124,** 243 (1929).
7. Koutsky, J. A., and R. J. Adler, *Can. J. Chem. Eng.,* **42,** 239 (1964).
8. Dean, W. R., *Phil. Mag.,* **4,** No. 7, 208 (1927).
9. *Ibid.,* **5,** No. 7, 673 (1928).
10. Cuming, H. G., *Aeronautical Research Council Reports and Memoranda No. 2880* (1952).
11. Dean, W. R., and J. M. Hurst, *Mathematika,* **6,** 77 (1959).
12. Truesdell, L. C., Jr., Ph.D. thesis, Case Inst. Technol., Cleveland, Ohio (1963).
13. White, C. M., *Proc. Roy. Soc.,* **A123,** 645 (1929).
14. Adler, M., *Zeits. Ang. Math. Mech.,* **14,** 257 (1934).
15. Thomas, G. B., Jr., "Calculus," p. 388, Addison-Wesley, Cambridge, Mass. (1956).

Manuscript received January 1, 1967; revision received April 1, 1969; paper accepted April 2, 1969. Paper presented at AIChE Detroit meeting.

APPENDIX A: EFFECT OF PITCH ON THE RADIUS OF CURVATURE

Consider a tube wrapped on a cylinder to form a helix such that the perpendicular distance from the cylinder axis to the tube center line is r. Since the tube cannot be superimposed upon itself, the center line of the tube must each turn be translated some distance h parallel to the axis of the cylinder. This distance must be equal to or greater than the tube's outside diameter. We will assume the tube is evenly wrapped so the angle of incline is always constant.

The tube center line forms a helix with a helical axis which coincides with the cylindrical axis. The radius of curvature of any point on this helical center line is $r + \frac{1}{r}\left(\frac{h}{2\pi}\right)^2$. The derivation of the magnitude and position of the radius of curvature of a helix is presented as an example in a text by Thomas (*15*).

Any point in the cross section of the tube will circumscribe a helix as the cross section is translated along the center line. Such a helix will also have an axis which coincides with the cylindrical axis. Thus, a general point in the tube cross section, a distance $r + x$ from the helical axis, has a radius of curvature $(r + x) + \frac{1}{(r+x)}\left(\frac{h}{2\pi}\right)^2 = r + aX + \frac{1}{r + aX}\left(\frac{h}{2\pi}\right)^2 \simeq r + aX + \frac{1}{r}\left(\frac{h}{2\pi}\right)^2$.

This expression is not of the form of the radius of curvature expression employed in the system Equations (3a) and (3b), namely $r + x = r + aX$. As long as the inclined distance h is small with respect to the helical circumference, however, the radius of curvature for a general point is very closely approximated by the expression $r + 1/r\left(\frac{h}{2\pi}\right)^2 + aX$. This form is readily adaptable to equation (3a) and (3b) by substituting $\frac{a}{r\left[1 + \left(\frac{h}{2\pi r}\right)^2\right]}$ for $\frac{a}{r}$.